Journal of Environmental Health Science and Engineering (2019) 17:219–232
https://doi.org/10.1007/s40201-019-00342-5

RESEARCH ARTICLE

Synthesis, characterization and photocatalytic application of Ag-doped Fe-ZSM-5@TiO_2 nanocomposite for degradation of reactive red 195 (RR 195) in aqueous environment under sunlight irradiation

Nasrin Aghajari[1] · Zahra Ghasemi[2] · Habibollah Younesi[1] · Nader Bahramifar[1]

Received: 12 September 2018 / Accepted: 21 January 2019 / Published online: 3 April 2019

Abstract

Background Most dyes have aromatic rings in their structures, which make them highly toxic for human being and aquatic life. Heterogeneous photodegradation using TiO_2 nanoparticles is one of the most applied methods used for dye removal. The wide band gap of TiO_2 nanoparticles disables its use of the visible light and thus the vast potential of sunlight. To overcome this deficiency, Ag doped TiO_2 nanoparticles were loaded on Fe-ZSM-5.

Methods Fe-ZSM-5@TiO_2-Ag photocatalyst was synthesized through sol-gel and hydrothermal methods to remove hazardous Reactive Red 195 (RR 195) from aqueous solution.

Results Pure phase of Fe-ZSM-5@TiO_2-Ag with specific surface area of 332 m^2/g was successfully synthesized. Formation of Ti-O-Ag functional group in the photocatalyst structure confirmed the nanocomposite form of the product. SEM and TEM images portrayed the synthesized zeolite and photocatalyst NPs in a size range of ≤100 nm with homogenous distribution of Ag doped TiO_2 on Fe-ZSM-5 surface. The band-gap energy of Fe-ZSM-5@TiO_2-Ag was calculated 1.97 eV at $\lambda = 630$ nm. Photocatalytic activity of the photocatalyst under natural sunlight was investigated through photodecomposition of RR 195 in an aqueous solution. The dye photodecomposition of about 98% was achieved at photocatalyst concentration of 400 mg/L, pH of 3, and dye concentration of 50 mg/L at ambient temperature after 120 min under sunlight using 0.5 ml of TiO_2 and silver ammonium nitrate. The photocatalyst reusability was found significant after 5 frequent cycles.

Conclusion The novel Ag-doped TiO_2-Fe-ZSM-5 nanocomposite with sunlight sensitivity can be a promising candidate to purify wastewater containing organic pollutants.

Keywords Sunlight-sensitive nanocomposite · Photocatalytic degradation · Reactive red (RR 195) 195 · Natural sunlight · Regeneration

Introduction

Waste effluents from textile, dyeing, printing, rubber, paper, plastic, and related industries contain various dyes. Most dyes have aromatic rings in their structures, which make them highly toxic, non-biodegradable, carcinogenic, and mutagenic for human being and aquatic life [1, 2]. Their colors also leaves visual pollution effects in the environment. The azo dye RR 195 is commonly used for textile dyeing industries. The dye contains reactive group which is often a heterocyclic aromatic ring substituted with chloride or fluoride and has maximum absorbance at 540 nm [3]. Dyes could not be easily destroyed via traditional treatments and their biological and biodegradation treatments are also difficult [4, 5]. Therefore, removal of various dyes from industrial wastewater before discharging them into natural water bodies is of high importance for environmental safety. There are different methods that can be used for textile wastewater treatments, such as Fenton, photo-Fenton, flocculation and coagulation, adsorption processes [2, 6–8], biological treatment [9–11], electrochemical techniques, ion exchange, Advanced Oxidation Processes (AOPs), and photcatalytic degradation under UV light. AOP

✉ Zahra Ghasemi
z.ghasemi@hormozgan.ac.ir; zghasemi446@yahoo.com

[1] Department of Environmental Science, Faculty of Natural Resources, Tarbiat Modares University, Noor, Iran

[2] Department of Fisheries, Faculty of Marine Science and Technology, University of Hormozgan, Bandar Abbas Postal Code: 7916193145, Iran

can be an alternative process for traditional wastewater treatments since providing a potential for a nonselective attack to organic matter [12]. The advantages of this technology include decomposition of most organic and inorganic compounds, such as water, carbon dioxide, and mineral acids, having no waste production, and avoidance of any problems at ambient temperature and atmospheric pressure [13]. Oxide matrices can be virtually produced by in situ AOPs resulting in highly reactive hydroxyl (OH^-) radicals with the help of primary oxidants like TiO_2, H_2O_2, UV, etc. These methods are very effective in removing the organic pollutants that resist biodegradation [14, 15]. Among various types of photocatalysts, TiO_2 has received much attention due to its favorable properties, such as being non-toxic, affordable, and sustainable for a long time, as well as photocatalytic properties for water and wastewater treatments and air pollution removal [16–18]. It is a white powder semiconductor with a wide band gap of 3.0–3.2 eV. [19]. TiO_2 photocatalyst initiates the oxidation process by absorbing the energy of a photon that is equal to or greater than the band gap width, through which an electron (e) of the Valence Band (VB) can be promoted to the Conduction Band (CB). The VB would then generate the vacancy electrons or holes (H^+), which can diffuse [20] throughout the solid followed by trapping or recombination. A small specific surface area and low absorption property are the limits to the effectiveness of photocatalytic TiO_2. The solution to these limits would be fixing TiO_2 on the surface of an adsorbent to increase the concentration of an organic material around the catalyst particles and thus enhance their efficiency and photodegradation [21]. Among the different supports for fixing TiO_2, zeolite has been recognized as the best support due to its porous structure and uniform pore size, regular channels, high surface area, high thermal stability, photochemical stability, high absorption capacity, environmentally and friendly nature [22]. It is supposed to have the ability of elevating the reaction rate by effectively separating the photogenerated electrons. Moreover, the excited electrons of TiO_2 band gap can be delocalized by it, a process which would then lead to minimized electron-hole recombination [23, 24]. Furthermore, the presence of zeolite as a support for TiO_2 photocatalyst would result in the maintenance of nearby dye molecules that increase the degradation rate [25]. Another problem with using TiO_2 as a catalyst is its efficiency of low-quantum light arisen by the electron-hole recombination. Its large band gap width disables its use of the visible light and thus the vast potential of sunlight. Alternatively, inert metal deposition on TiO_2 surface would lead to improved performance by reducing the recombination of electrons trapped in the holes and helping in surface load transfer [26]. Metal ion doping of TiO_2 would sensitize it to visible light as the original spectra of sunlight [27]. Generally, TiO_2 doped with metal ions in the redox potential-generated radicals improve and expand the light absorption spectra. Additionally, electron-trapping metal ions would contribute to the reduction of electron-hole recombination [28]. Changes in the light absorption and absorption capacity of dye molecules on the catalyst surface, as well as increases in the speed of interfacial charge transfer would affect the photocatalytic activity of TiO_2. The conduction band overlap of Ti (3d) with the d orbitals of transition metals results in the red shift transfer of TiO_2 band edge. Modified photocatalyst, such as TiO_2 doped with Ag, have excellently repeatable adsorption capabilities of visible light [29]. In addition, as shown by our previous studies [30, 31], significant photodegradation efficiency of organic pollutants using Fe-ZSM-5@TiO_2 indicates good potential of this technique as a treatment system for real petroleum refinery wastewater. The results showed that the incorporation of iron in ZSM-5 zeolite can make it a photocatalyst [30–32]. The excited state of iron formed in Fe-ZSM-5 framework as a support of TiO_2 plays the same role as that of photogenerated electron-hole pairs on the semiconductors. Therefore, the conduction band overlap of Ti (3d) with the d orbitals of iron in Fe-ZSM-5 framework and electron transfer of Fe^{3+} (d) to TiO_2 conduction band would decrease the band gap of TiO_2 and increase visible light absorption ability of photocatalyst [30, 31, 33].

Accordingly, the aim of the present work was to develop Fe-ZSM-5@TiO_2-Ag nanocomposite by imprinting TiO_2 and Ag in the synthesized Fe-ZSM-5 zeolite structure and investigate its photocatalytic activity for removing RR 195 from aqueous solution under sunlight at ambient temperature. Based on our previous studies [30, 31], the goal of the present study was to develop a novel complex assembly with high photocatalytic activity under sunlight. It is believed that the unique characteristics of Fe-ZSM-5 as support of TiO_2 and Ag doping of it would effectively enhance the visible light absorption of this type of zeolite based photocatalyst by reducing the band gap.

Materials and methods

Synthesis of Fe-ZSM-5 zeolite

The mole ratio of the starting hydrothermally- synthesized solution of Fe-ZSM-5 zeolite was $10SiO_2$:0.0493 Fe_2O_3:1TPABr:$3Na_2O$:$500H_2O$ [30]. First, 3.03 g of sodium silicate (Na_2SiO_3) (Carlo Erba) and 1.48 g tetrapropylammonium bromide (TPABr) (Merck) were separately dissolved in deionized water, while the latter was heated at 50 °C for 20 min. Then, the two solutions were mixed together and stirred for 15 min. After getting clear to ensure complete mixing of the solutions, this combined solution was slowly poured into another solution of iron (III) nitrate nonahydrate (98%, Sigma-Aldrich) and deionized water (24.9 mL) and vigorously stirred. Upon transferring the

resultant mixture into a stainless steel autoclave, it was vertically placed in an oven to be heated at 170 °C for 72 h. The obtained solid product was then filtered and washed with adequate distilled water to reach a pH of 7.0. Finally, the 4 h calcination of the product at 450 °C with a heating rate of 3 °C/min was followed by drying it in an oven at 110 °C for 24 h [30]. The schematic diagram of different stages of hydrothermal synthesis of Fe-ZSM-5 zeolite is presented in Fig. 1.

Synthesis of Fe-ZSM-5@ TiO_2 photocatalyst

An ammonium chloride solution (Merck ACS reagent grade) was first utilized to convert the Na-form of the synthesized Fe-ZSM-5 into its H-form for Fe-ZSM-5@TiO_2 preparation [30]. Then, hydrochloric acid was employed to catalyze tetra–n-butyl orthotitanate ($Ti(OC_4H9)_4$, TBOT) hydrolysis in dry 2-propanol so as to load the nanometer size of TiO_2 onto the H-form of Fe-ZSM-5 via the sol-gel technique. The typical TBOT was added dropwise to the obtained solution and vigorously stirred at 0 °C for 6 h after dissolving it in 30 mL of 2-propanol and subsequently 1 mL of 0.1 M HCl (37%, Merck). The final solution was mixed with Fe-ZSM-5 and vigorously stirred at 25 °C for 4 h. The solvent removal under vacuum via rotary evaporation and drying at 110 °C were followed. Finally, TiO_2 crystallinity was induced in zeolite by calcining the photocatalyst at 550 °C at a heating rate of 5 °C/min under air for 4 h [34].

Synthesis of Fe-ZSM-5@TiO_2-ag photocatalyst

The outer layer of Ag was doped on the surface of Fe-ZSM-5@TiO_2 using a combination of the sol-gel process, chemical reduction method, and a hydrothermal approach. In this synthesis, 0.2 g of the H-form of Fe-ZSM-5 was dispersed in a mixture of 30 mL of 2-propanol and 0.5 mL of TBOT and then, 0.48 mL of 0.1 M silver nitrate ($AgNO_3$) solution was added to the suspension. Afterwards, 0.1 M hydrazine hydrate

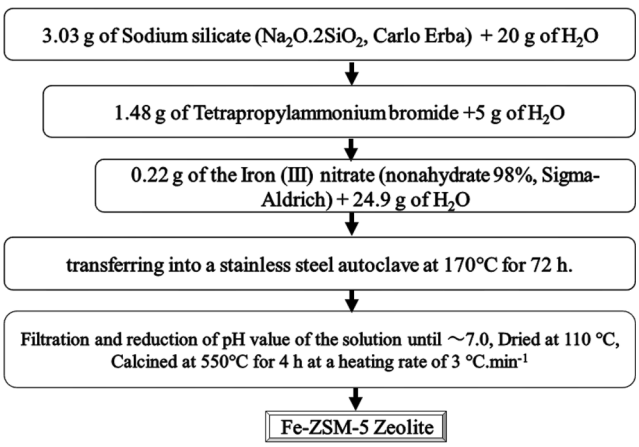

Fig. 1 The schematic diagram of different stages of hydrothermal synthesis of Fe-ZSM-5 zeolite

($N_2H_4.H_2O$) solution (1 mL) as a reducing agent was added dropwise to it and vigorously stirred. The final suspension was transferred into a 50 mL Teflon-coated steel autoclave, which was then sealed and kept at 160 °C for 6 h. After filtering the obtained composites, they were washed with ethanol and distilled water. Finally, they were dried at 60 °C for 6 h. The samples with different TiO_2 loading contents were selected to examine the effect of TiO_2 content on the photodegradation activity of the synthesized photocatalyst. At this stage, 0.25, 0.5, 0.75, and 1 mL of TBOT per 0.2 g of Fe-ZSM-5 zeolite was used, while all the variables were considered to be fixed. In addition, different concentrations of 0.1 M $AgNO_3$, including 0.25, 0.5, 0.75, and 1 mL per 0.2 g of Fe-ZSM-5 zeolite were selected to examine the effects of Ag content on the photodegradation activity of the synthesized photocatalyst under sunlight. The schematic diagram of different stages of the synthesis of Fe-ZSM-5@TiO_2-Ag is illustrated in Fig. 2.

Photocatalyst characterization

The powder XRD analyses of Fe-ZSM-5 zeolite, Fe-ZSM-5@TiO_2, and Fe-ZSM-5@TiO_2-Ag photocatalysts were performed by a PW 1800 Philips X'Pert diffractometer using CuKa radiation. The X-ray wavelength was derived from a copper anode (CuKa) and the data were collected in a 2θ range of 5–70° with a step size of 0.02°/s. The synthesized materials were also characterized by SEM (Philips, XL30) operated at 30 kV and FT-IR spectrophotometer (Shimadzo, FTIR1650, Japan) in a wavenumber range of 400–4000 cm^{-1}. A conventional volumetric apparatus (Bel Japan, BELSORP 28SA) was utilized to measure the adsorption/desorption isotherms of nitrogen at 77 K. The specific surface areas of the products were calculated via the Brunauer-Emmett-Teller (BET) equation. Finally, a JASCO V-650 spectrophotometer (Japan) was employed to record the UV-Vis absorption spectra of the products within a wavelength range of 200–1000 nm.

Solar experiments and photocatalytic activity measurements

Despite an artificial light source with a constant light, sunlight source includes variable light intensities during the hours, days, and seasons of the year. The variables of sunlight intensity over time were measured in sunny days using a light meter (LX-1108 Lutron). The total time of the experiments was 2 h between 11:30 am and 2 pm providing maximum sunlight intensity during the day in July and September. The average sunlight radiations during the mentioned period in late July, early August, and early September had a range of 2000–3500 lx. RR 195 degradation was investigated using its different initial concentrations in the range of 25–150 mg/L. The experiments were carried out using 100 mL of RR 195 solution at the desired concentrations and adjusted pH values of

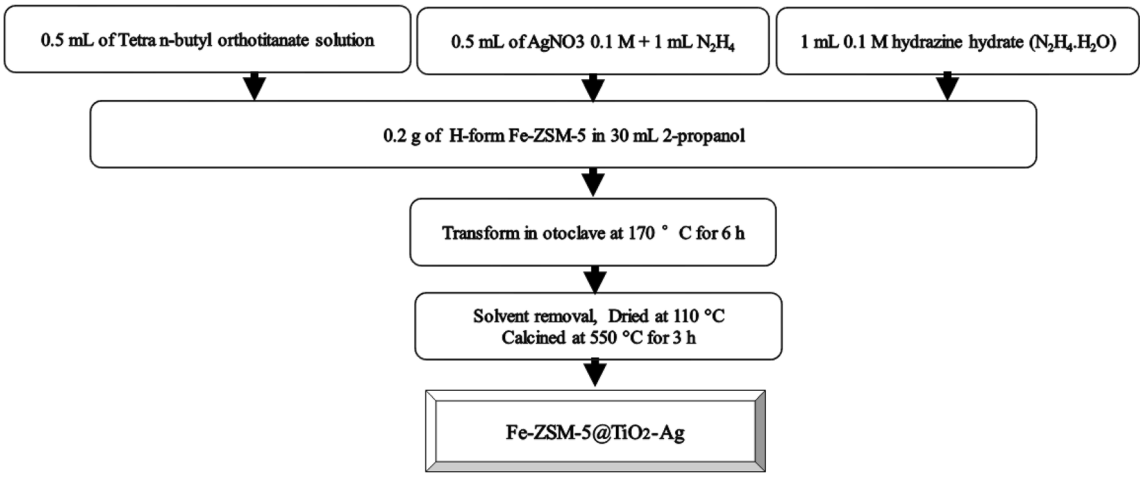

Fig. 2 The schematic diagram of different stages of the synthesis of Fe-ZSM-5@TiO_2-Ag

the experimental solution. To adjust its pH, the effects of the pH range of 2.0–9.0 on RR 195 removal were examined. Upon adding the photocatalyst, the effects of the different photocatalyst concentrations in the range of 100–500 mg/L were studied. The samples with different TiO_2 loading contents and different concentrations of 0.1 M $AgNO_3$ were selected to examine the effect of TiO_2 and Ag content on the photodegradation activity of the synthesized photocatalyst, respectively. After adding an appropriate amount of the photocatalyst, the aqueous slurry was stirred in the dark for 30 min to equilibrate the adsorption and desorption between RR 195 and the photocatalyst. Then, it was irradiated under natural sunlight on clear sunny days at ambient temperature. The sampling time was considered to be once every 15 min. The samples were transferred to the laboratory where their dye concentrations were measured at 540 nm using the Palintest Photometer 8000 (UK). At least, 3 replicate samples were used for the whole analyses and the average values of which were then reported.

Results and discussion

Physicochemical properties of ag-doped Fe-ZSM-5@TiO_2 nanocomposite

XRD was used to investigate the phase structures of the samples. The XRD patterns of Fe-ZSM-5, Fe-ZSM-5@TiO_2, and Fe-ZSM-5@TiO_2-Ag are shown in Fig. 3a, b, and c. The peaks at 2 = 7.94, 8.01, and 8.90° and 2 = 23–25° respectively corresponding to Fe-ZSM-5 and MFI frameworks confirmed the presence of Fe-ZSM-5 crystal phase [35]. The characteristic peak of TiO_2 anatase form appeared at 2 = 25.3°. The 3 sharp peaks of 38.47°, 44.65°, and 64° were corresponding to the crystal planes of (111), (200), and (220) exhibited by Ag diffraction pattern, respectively. A match was

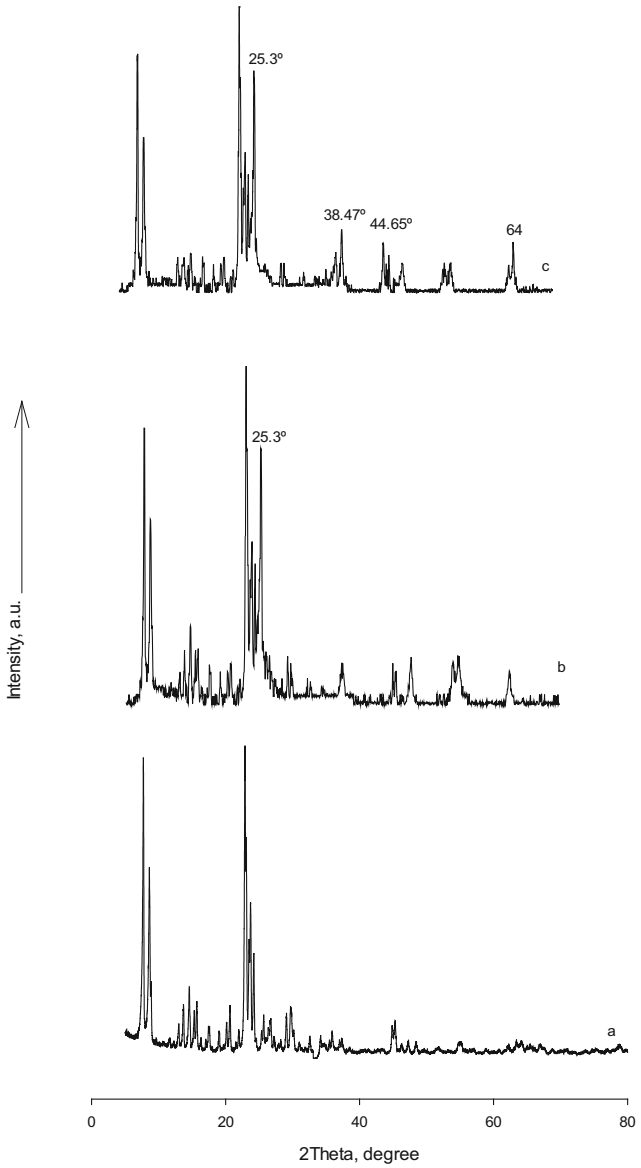

Fig. 3 XRD patterns for **a** Fe-ZSM-5, **b** Fe-ZSM-5@TiO_2 and **c** Fe-ZSM-5@TiO_2-Ag

found for the customary Bragg reflections of Face-Centered Cubic (FCC) silver, thus confirming the purities and identities of the obtained precipitates based on the standard data of JCPDS Card File (40783) [36].

The surface morphologies and size uniformities of Fe-ZSM-5 and TiO_2-doped Ag nano-particles (NPs) were studied through SEM analysis (Fig. 4a, b, and c). The SEM image of zeolite shown in Fig. 4a presents the cube-like crystals with a clean and smooth surface. The synthesized zeolite had a narrow range of particle size (≤1 μm). As shown in Fig. 4b, the small particles located on the cubic particles of Fe-ZSM-5 are related to the nano-TiO_2 anatase. TiO_2 particles only adhered to zeolite surface and cavities, but did not appear inside the pores. The nano-TiO_2 particles were well distributed on its surface and consequently unsmoothed it. Its particle size showed a slight enhancement after TiO_2 loading. The SEM image revealed the attaching of TiO_2 NPs to zeolite surface, while no changes had occurred to the typical zeolite morphology after TiO_2 loading.

Figure 5a and b portray the TEM images of the synthesized zeolite and photocatalyst NPs in a size range of ≤100 nm with their homogenous distributions on Fe-ZSM-5 surface. TiO_2 has been deposited in zeolite structure via sol-gel method so that a homogenous layer of the NPs with a uniform particle size and shape has surrounded zeolite crystals with a thickness of about 25 nm. As it is clear from the TEM images, zeolite particles have undergone a slight increase of size after the NP deposition. TEM images clearly displayed the coated NPs and hence, Fe-ZSM-5 synthesis based on TiO_2 dopinged with Ag was successful [37, 38]. It is noteworthy to mention that TiO_2 NPs doped with Ag provided a highly stable condition inside zeolite structure without breaking off, which could be the result of electron transmission between the two phases. The results suggested that the synthesized nanocomposite was in a good crystalline quality.

The N_2 adsorption and desorption isotherms of Fe-ZSM-5 (Fig. 6a) indicated the presence of zeolite structure and an adsorption/desorption curve with the overlapping like ~.

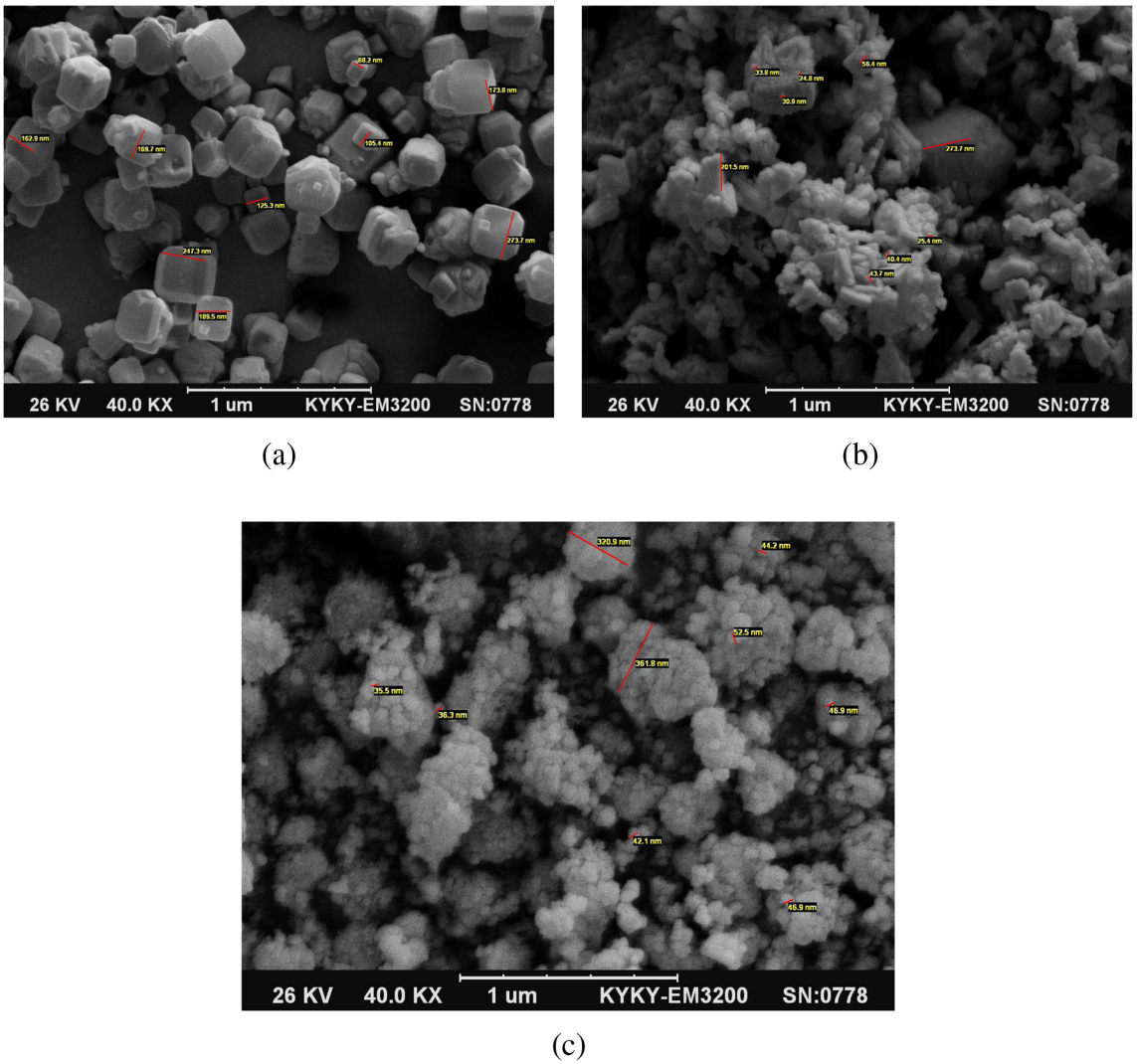

Fig. 4 SEM morphology for **a** Fe-ZSM-5, **b** Fe-ZSM-5@TiO_2 and **c** Fe-ZSM-5@TiO_2-Ag

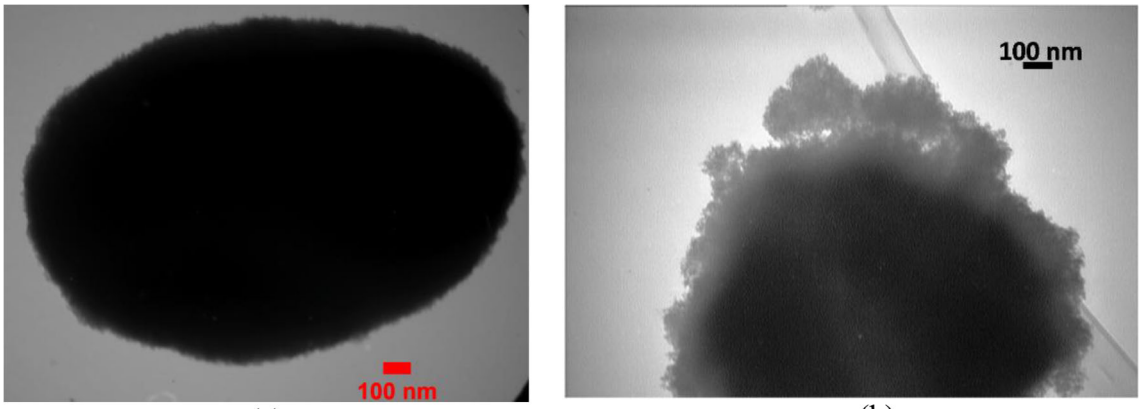

Fig. 5 TEM morphology for **a** Fe-ZSM-5, **b** Fe-ZSM-5@TiO_2-Ag

Based on IUPAC classification, the adsorption and desorption isotherms of Fe-ZSM-5 appear in the form of a type-II isothermal adsorption capable of increasing the volume of N_2 adsorption at relatively low pressures. This indicated that the zeolite sample had a pore size distribution in the microporous region [39]. The BET surface area, pore size, and volume are summarized in Table 1. It can be observed that the adsorption and desorption isotherms of ZSM-5, Fe-ZSM-5 @TiO_2, and Fe-ZSM-5@TiO_2-Ag (Fig. 6a, b, and c) are not the same for a specified region of relative pressures. The N_2 adsorption and desorption isotherms of Fe-ZSM-5@TiO_2 and Fe-ZSM-5@TiO_2-Ag represent a type-IV isotherm curve with a hysteresis loop. The adsorption and desorption branches are parallel, which is the characteristic of an H_2-type loop commonly exhibited in mesoporous materials [40]. After loading TiO_2 onto Fe-ZSM-5, the photocatalyst surface area enhanced compared to that of zeolite, which could be due to the growth of TiO_2 NPs and their depositions on the photocatalyst surface without blocking zeolite pore system. Immobilization and crystallization of TiO_2 on zeolite structure could form a microporous structure capable of increasing the pore volume of TiO_2–zeolite nanocomposites [39] (Table 1). Ag doping led to the reduction of the photocatalyst surface area with an average pore diameter of larger than those of Fe-ZSM-5 and Fe-ZSM-5@TiO_2. In addition, the micropore volume of the synthesized photocatalyst decreased compared to those of Fe-ZSM-5 and Fe-ZSM-5@TiO_2. Immobilization of Ag-doped TiO_2 crystallites on the external surface of zeolite blocked zeolite pores and resulted in the micropore volume attenuation. Investigation of the specific surface area of Ag-doped Fe-ZSM-5@TiO_2 before and after surface modification with Ag using N_2 adsorption/desorption technique showed that more increase in the silver amount of Fe-ZSM-5@TiO_2 photocatalyst can cause more decrease in the specific surface area of the Ag-doped photocatalyst. This could be due to the blocking of Fe-ZSM-5@TiO_2 pores and channels via Ag doping [41, 42].

7The FT-IR spectra of pure Fe-ZSM-5, Fe-ZSM-5@TiO_2, and Fe-ZSM-5@TiO_2-Ag nanocomposites are presented in Fig. 7a, b, and c. The FT-IR spectra of the precursor revealed the strong OH stretching and absorbing bands resulting from the vibration of silanol groups (Si–OH), as well as adsorbing of water molecules at 3500 and 3646 cm^{-1} [43, 44], which had been induced by the interaction between Si groups in zeolite and water molecules. The peaks observed at 792 and 1300–800 cm^{-1} were due to the asymmetric or unsymmetric stretching vibrations of (T–O–T) = Si, Fe, and Ti in the zeolite and photocatalyst network. The vibrational peak at 546 cm^{-1} confirmed the Quintet ring structure of ZSM-5 zeolite [44]. Vibrations of T–O (T = Si, Fe, and Ti) asymmetric bending, asymmetric stretching vibrations, and symmetric stretching peak of TO_4 group were observed at 462, 1008, and 1680 cm^{-1}, respectively. The vibrations at 859 and 1087 cm^{-1} were attributed to the stretching vibration of Ti–O–T (T = Si, Fe, and Ti) resulted from TiO_4 area [45, 46]. Transition metal Ag nanoclusters are generally more strongly attached on oxide supports such as T–O (T = Si, Fe, and Ti) that allow the formation of O-rich metal-support interfaces [47]. The band at 730 cm^{-1} could be possibly due to the asymmetrical stretching vibration of Ti–O–Ag [48] which confirms that the synthesized nanocomposit is not a mechanical mixture of TiO_2 anatase, Ag, and zeolite. After TiO_2 deposition in zeolite structure, the peak intensity at 3500 cm^{-1} declined, thus suggesting replacement of a significant amount of O–H bond attached to silanol groups with O–Ti. The deposition destroyed O–H bond attached to silanol groups, while H was replaced by Ti. The peak identified at 1654 cm^{-1} was ascribed to the bending vibration of OH [22, 34]. The private peak of Ti–O (Ti–O–Si and Ti–O–Fe) bond was observed at the areas of 850 and 1087 cm^{-1} [49, 50]. The absorption band at 897 cm^{-1} in the FT-IR spectrum of the synthetic photocatalyst represented TiO_2 phase. These observations indicated that bonds had been made between Ti and the nanocomposite structure and proved that the microporous layer of TiO_2 crystallites had been formed in zeolite structure [39]. Based on the formations of new bonds, it was deduced that the synthesized photocatalyst was not simply a mechanical

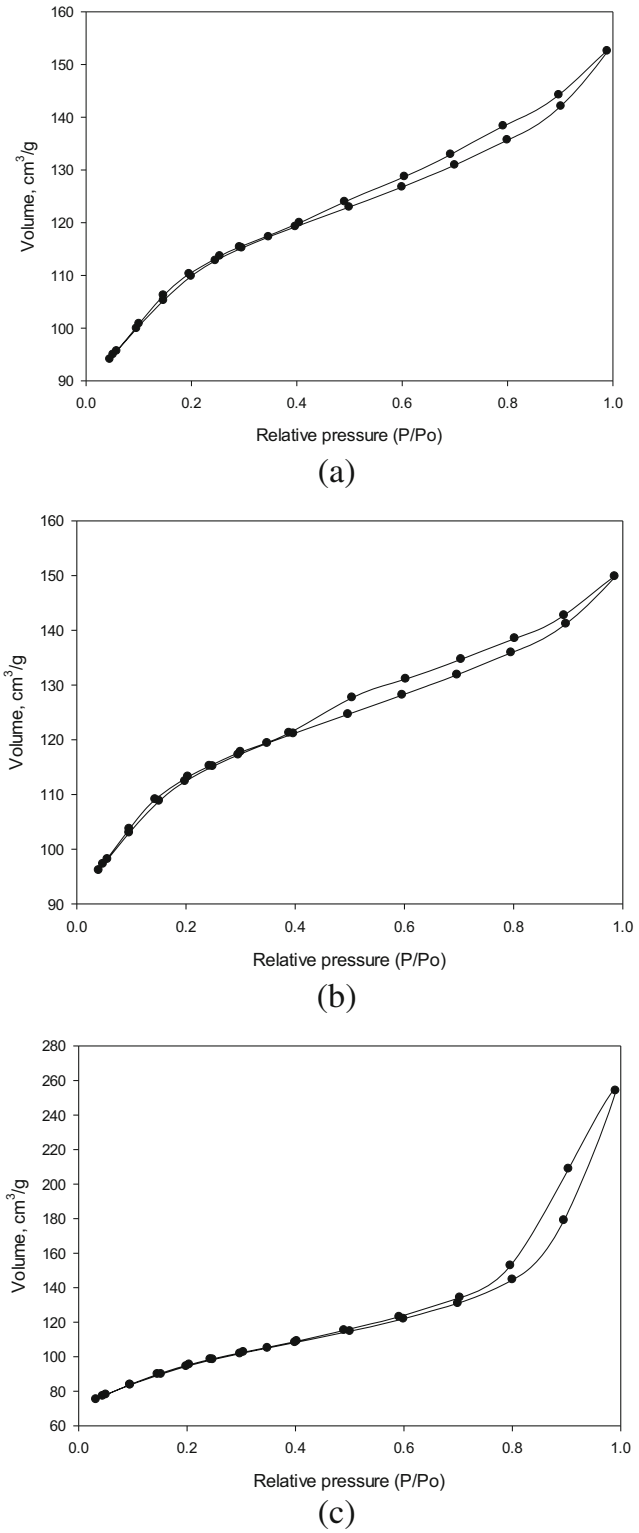

Fig. 6 The N_2 adsorption/desorption isotherm of synthesised **a** Fe-ZSM-5, **b** Fe-ZSM-5@TiO_2 and **c** Fe-ZSM-5@TiO_2-Ag

mixture of TiO_2 anatase, Ag, and zeolite, but a new nanocomposite.

In UV-Vis spectroscopy, when the material is placed under irradiation, electrons are transmitted from the atomic or molecular orbitals of a lower energy to a higher energy. The electron transfer process may occur at the interfaces between metal ions and organic and inorganic molecules. [51] Fig. 8a, b, and c display the UV–Vis spectra of the products measured within the regions of 200–1000 nm. The absorption edges of Fe-ZSM-5@TiO_2 and Fe-ZSM-5@TiO_2-Ag nanocomposites were at 560 and 630 nm, respectively. The changes in the band gap energies of the synthetic photocatalysts were calulated according to Equation 1 [52]:

$$\text{Band gap energy } (E) = \frac{hC}{\lambda} \quad (1)$$

where h is Plank's constant equal to $6.626*10^{-34}$ J sec; C is the speed of light equal to $3.0*10^{8}$ m/s; and λ is the cut-off wavelength in a meter scale.

The band gap energies with the absorption edges of λ = 560 and 630 nm were calculated to be equivalent to 2.22 and 1.97 eV, respectively. The absorption features suggested the possible activation of Fe-ZSM-5@TiO_2-Ag photocatalytic activity by visible light.

Table 1 Surface texturing data of as-prepared ZSM-5 zeolite, Fe-ZSM-5@TiO_2 and Fe-ZSM-5@TiO_2-Ag photocatalyst

Properties	Fe-ZSM-5	Fe-ZSM-5@TiO_2	Fe-ZSM-5@TiO_2-Ag
S_{BET}, m^2/g	380	388	332
dp, nm	1.67	2.38	4.75
V_T, $cm^3\ g^{-1}$	0.24	0.23	0.39
V_{mp}, $cc.g^{-1}$	0.19	0.19	0.09
$\%V_{mp}$	78.48	81.47	23.10

Photocatalytic degradation of RR 195 under sunlight irradiation

In order to examine the effect of adsorption by photocatalyst on RR195 photodegradation, experiments were conducted both in the absence (dark condition) and presence of sunlight at photocatalyst concentration of 300 mg/L and pH of 3.0 for 120 min. The RR195 removal at initial dye concentration of 50 mL/L, pH of 3 and photocatalyst concentration of 300 mg/L under absence of photocatalyst, absence of sunlight and presence of both photocatalyst and sunlight are illustrated in Fig. 9. Fe-ZSM-5@TiO_2-Ag was only used as an absorbent, while the reactor was kept in dark for 120 min to reach a steady state. A very low amount of the dye was removed by Fe-ZSM-5@TiO_2-Ag under the dark condition at pH value of 3, while maximum dye removal of 98% was achieved under sunlight with the same operational condition. The reason of low removal efficiency under dark condition may be due to very low adsorption of RR195 by Fe-ZSM-5@TiO_2-Ag surface.

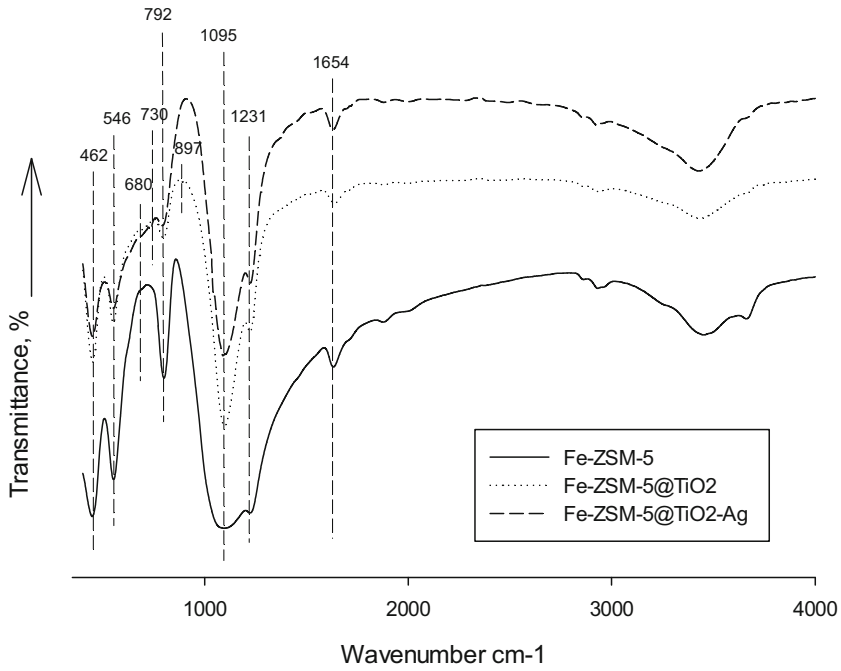

Fig. 7 The FT-IR spectra in the 400–4000 cm^{-1} range of prepared Fe-ZSM-5 zeolite (**a**), Fe-ZSM-5@TiO_2 (**b**) and Fe-ZSM-5@TiO_2-Ag (**c**)

In order to examine the effect of sunlight on RR195 photodegradation, experiments were conducted in the presence of sunlight and absence of photocatalyst under the above condition. The RR195 removal of about 6 % was achieved under the mentioned condition. The results illustrated that photodegradation process played a more important role than adsorption process. All these results indicate that in the absence of photocatalyst, there is no radical generation to degrade RR195. On the other hand, in the absence of sunlight, photo-excitation of Fe-ZSM-5@TiO_2-Ag cannot be occurred. Therefore, both sunlight and photocatalyst are needed for effective removal of RR195. This result is in agreement with previous reports [30, 31, 53].

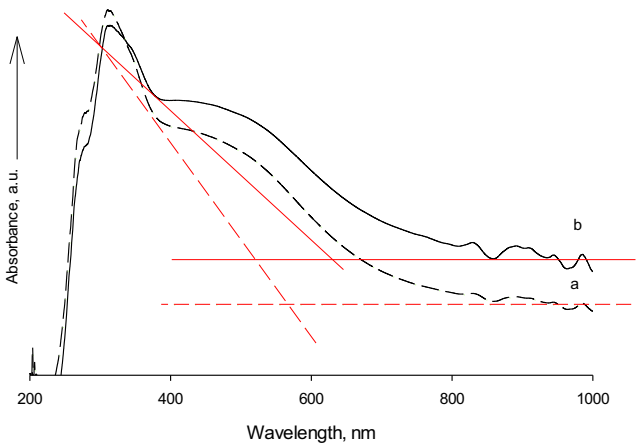

Fig. 8 The UV-Vis absorption spectra of prepared **a** Fe-ZSM-5@TiO_2 and **b** Fe-ZSM- 5@TiO_2-Ag

Effect of pH

pH is a main factor affecting the degradation rates of some organic compounds during the photocatalytic process and plays a significant role in OH radical generation [54]. Moreover, pH of a solution is the major influential parameter on adsorption since affecting the chemical properties of both the dye molecules and the adsorbent [7, 55]. The effects of the pH range of 2.0–9.0 on the removal of RR 195 were investigated and illustrated in Fig. 10. At a pH value of 3, the dye removal effectiveness was more than neutral and thus more playable. The

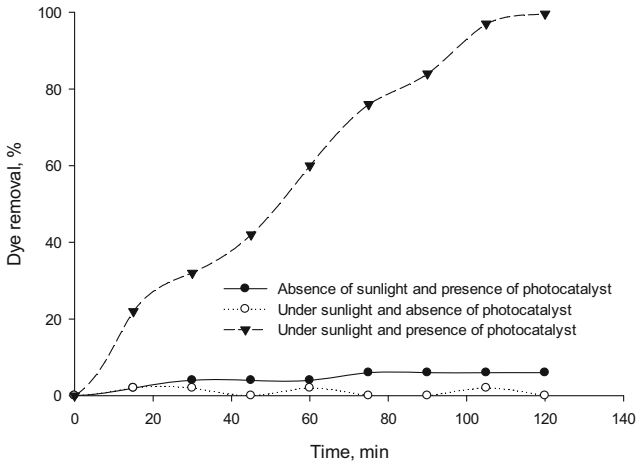

Fig. 9 The RR195 removal at initial dye concentration of 50 mL/L, pH of 3 and photocatalyst concentration of 300 mg/L under **a** absence of photocatalyst, **b** absence of sunlight and **c** presence of both photocatalyst and sunlight

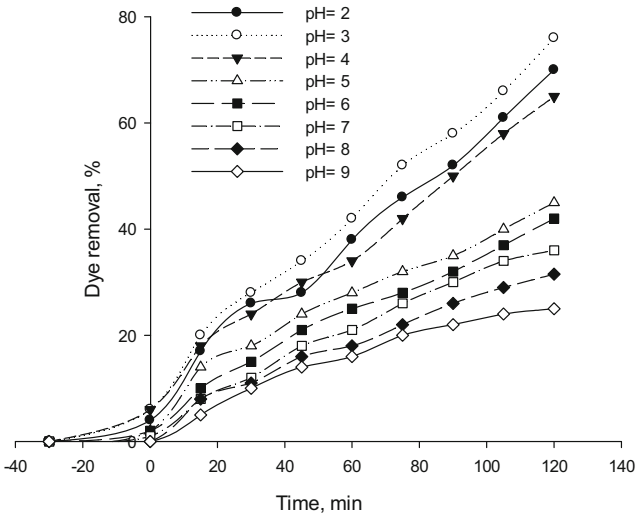

Fig. 10 The effect of pH on RR195 photodegradation using Fe-ZSM-5@TiO_2-Ag (initial dye concentration of 50 mL/L, photocatalyst concentration of 300 mg/L)

removal rate was decreased by increasing pH. Accordingly, the highest and the lowest removal rates were obtained at the pH values of 3 and 9, respectively. Acidic media provide higher degradation rates, which decrease with increasing pH. The results are in accordance with the results reported by Safari et al. [18], who studied photocatalytic degradation of tetracycline using nanosized TiO_2 under UV irradiation. pH effect was related to the catalyst surface ionization, zeolite behavior in the alkaline and acidic media [56], and the dye form and structure consisting of acids and amines. Its efficiency could change due to the release of protons via photooxidation and reversible protonation of TiO_2 surface [21]. To explain the mechanism of pH effect on the adsorption, it is necessary to first identify the surface charge on the adsorbent and adsorbate. The isoelectric point of TiO_2 where zeta potential equals zero is 6.4 [30]. Due to the H-bond formation between the catalyst protons and a single pair of electrons on the dye amino group in an acidic solution, the synthesized photocatalyst could strongly adsorb the dye. Therefore, a quick photodegradation rate would be achieved in acidic solutions under sunlight compared to the cases of neutral or alkaline pH solutions [57]. RR 195 is an anionic dye containing a negatively charged group. The higher adsorption capacity at a lower pH value might be due to the electrostatic attraction between the negatively charged molecules of the dye and positively charged molecules of Fe-ZSM-5@TiO_2-Ag. Therefore, the removal process was much more effective in an acidic compared to alkaline condition. These results are similar with results reported by Hemmati Borji et al. [17], who found that phenol degradation was much more effective in an acidic compared to alkaline condition using Fe(III)-doped TiO_2 and TiO_2 nanoparticles.

Effect of the catalyst concentration

To determine the optimal loading of the catalyst, RR 195 degradation was studied by using various concentrations of the catalyst within the range of 100–500 mg/L. The results are presented in Fig. 11. By increasing the catalyst concentration from 100 to 300 mg/L, the dye discoloration efficiency was observed to enhance. As shown in Fig. 11, an increase in the catalyst concentration results in an enhanced initial rate until it reaches its maximum value and remains almost constant at any higher concentrations. The optimum concentration of the catalyst for the highest degradation efficiency of RR 195 was at 500 mg/L under the experimental conditions specified in Fig. 11. The numbers of the absorbed photons and adsorbed dye molecules were increased by enhancing the catalyst concentration leading to an elevated degradation rate [19]. Enhancement of the catalyst amount resulted in the increased numbers of hydroxyl and superoxide radicals caused by enhanced active sites on the photocatalyst surface [58]. The results are in accordance with those obtained by other researchers who studied the effect of TiO_2 concentration on the degradation of other organic pollutants [18, 59, 60]. In a study performed by Safari et al. [18], the degradation rate constants of tetracycline degradation increased with increasing TiO_2 density and declined slightly at a very high TiO_2 concentration under UV irradiation.

Effect of the initial RR 195 concentration

The initial concentration effect of the dye solution on its photocatalytic degradation was an important part of this study. To this goal, varied initial concentrations of RR 195 in a range of 25–150 mg/L were considered. The photodegradation percentage was reduced by enhancing the initial concentration

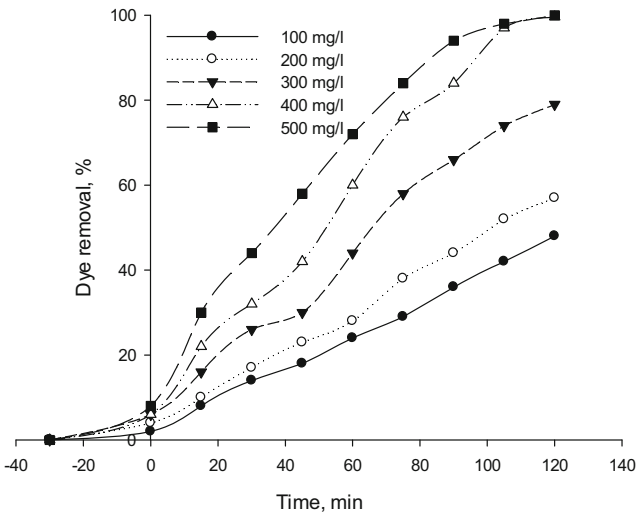

Fig. 11 Effect of the photocatalyst concentration on RR195 photodegradation using Fe-ZSM-5@TiO_2-Ag (initial dye concentration of 50 mL/L, pH of 3)

of the dye solution as represented in Fig. 12. The highest and lowest removal rates were achieved at the dye concentrations of 25 and 150 mg/L, respectively. Hydroxyl radicals have a very short lifetime of only a few nanoseconds and thus, they find the opportunity for reaction only at or near the locations of their formations [61]. This behavior can be explained by the greater adsorption of organic substances on the photocatalyst surface as the initial concentration is elevated [31] and thus, the dye ions cover the active sites in the photocatalyst structure. As a result, •OH radical generation on the photocatalyst surface is lowered. In addition, decreased number of photons are resulted from their interception prior to reaching the photocatalyst surface, thus leading to a reduced degradation percentage [62, 63]. Also, the effect of UV screening on the dye can be another possible reason for achieving such a result. Instead of TiO_2 particles, the dye molecules may significantly absorb UV at a high concentration, which causes the reduced concentrations of •OH and O_2• − and decreased efficiency of the catalytic reaction [56]. Consequently, the enhanced initial concentration of the dye would result in the increased requirement of the catalyst surface for degradation. These results are similar with results reported by Safari et al. [18], who studied tetracycline degradation using TiO_2 under UV irradiation. They found that the tetracycline degradation rate constants decreased with increase of the initial concentration of it. In another study, Hemmati Borji et al. [17] reported that photocatalytic degradation efficiency of Fe(III)-doped TiO_2 and TiO_2 nanoparticles decreased with increase in initial concentration of phenol.

Effect of ag content

The degradation stability and efficiency have been shown to be improved by the promising Ag-modified photocatalyst. The interfacial transfer of charges can be promoted by allowing noble metals like Ag to precipitate on TiO_2 surface, which acts as a trap for electrons and thus slows down the electron-hole pair recombination. The photocatalytic efficiency can be enhanced under visible light [64]. As it is illustrated in Fig. 13, by increasing the Ag content of the photocatalyst, the dye removal increases up to an optimum amount of Ag and then decreases. Table 2 summarizes the effect of different Ag contents of the photocatalyst on RR 195 removal percentage. By trapping electrons, Ag can effectively facilitate electron-hole separation and enhance electron production on TiO_2 surface, thus increasing the photocatalytic activity. Silver doping more than its optimum content induces a collection of silver particles, increases the electron-hole recombination centers, and ultimately reduces the photocatalytic efficiency [65]. In this study, 0.5 mL of 0.1 M $AgNO_3$ was considered as an optimum amount. Under sun radiation, TiO_2 NPs and silver were both promoted to generate electron-hole pairs. The electrons and holes generated in TiO_2 and silver reacted with water and produced Reactive Oxygen Species (ROS). The photocatalytic activity of the TiO_2 nanostructure in the presence of pure sunshine would be increased by doping Ag particles with it and facilitating electron movement via their absorption. In addition, the synthesized photocatalyst was composed of Fe-ZSM-5, which had Fe content. Fe can play a role as both an electron injector and a hole trap. The electron-absorbing NPs would stop the electron-hole pair recombination and thus greatly increase the photocatalytic activity. At the same time, O_2 generated from Ag made a great amount of the radical form of OH^+, which improved the photocatalytic activity under sunlight. Therefore, the photocatalytic activity could be increased by the Ag-doped TiO_2 based on zeolite under sunlight since being in the range of silver quantum dots [66].

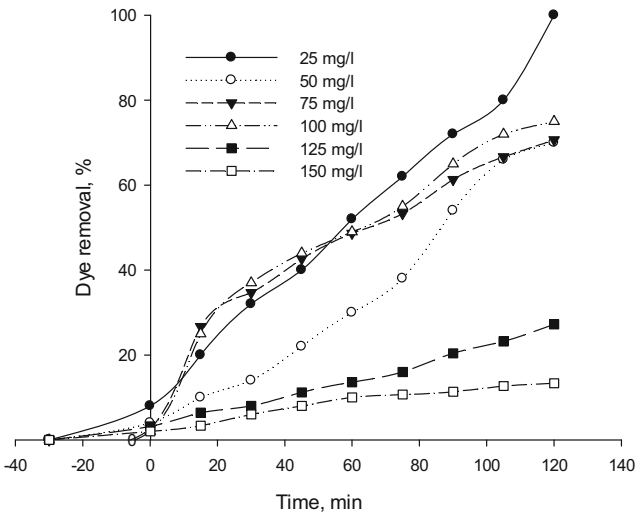

Fig. 12 Effect of initial dye concentration on RR195 photodegradation using Fe-ZSM-5@TiO_2-Ag (initial dye concentration of 50 mL/L, pH of 3, photocatalyst concentration of 300 mg/L)

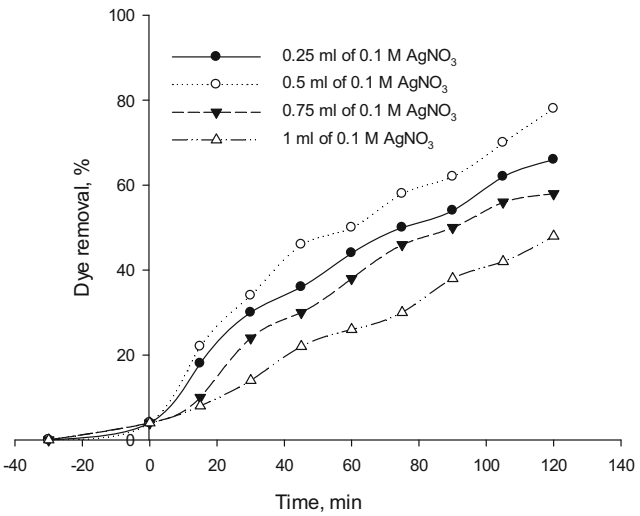

Fig. 13 Effect of silver content on RR195 photodegradation using Fe-ZSM-5@TiO_2-Ag (initial dye concentration of 50 mL/L, pH of 3, photocatalyst concentration of 300 mg/L and 0.5 mL of TBOT)

Table 2 Effect of different Fe-ZSM-5@TiO_2-Ag compositions on RR 195 removal percentage (initial dye concentration of 50 mL/L, pH of 3, photocatalyst concentration of 300 mg/L)

Sample	TiO_2 loading (mL of TBOT)	silver content (mL of 0.1 M $AgNO_3$)	RR 195 removal (%)
Fe-ZSM-5@TiO_2-Ag	0.25	0.5	66
	0.5	0.5	78
	0.75	0.5	62
	1	0.5	54
	0.5	0.25	66
	0.5	0.75	58
	0.5	1	48

As illustrated in Fig. 13, the dye removal decreases at the 0.1 M $AgNO_3$ amount of higher of 0.5 mL. Ag particle deposition of higher than an optimum amount might reduce photon absorption by TiO_2 and consequently provide electron-hole recombination centers, thus negatively affecting the photocatalysis efficiency. Nevertheless, the photocatalytic efficiency would be lowered by excessive Ag doping since leading to Ag particle conglomeration and photogenerated electron-hole recombination.

Effect of TiO_2 loading

The samples with different TiO_2 loading contents were selected to examine the effect of TiO_2 content on the photodegradation activities of the synthesized photocatalysts. Determination of TiO_2 to fe-ZSM-5 and Ag optimum ratio would reduce the required cost. As Fig. 14 shows, the removal efficiency increases by enhancing the TiO_2 content of the photocatalyst. In addition, Table 2 summarizes the effect of different photocatalyst composition on RR 195 removal percentage. As the TiO_2 content of the photocatalyst enhances, the number of active sites and subsequently, the generation of hydroxyl radicals ($OH^{\bullet}$) would be increased. This trend continues up to 0.5 mL of TBOT, while the removal efficiency decreases at its higher concentrations. It might be due to TiO_2 aggregation on Fe-ZSM-5 surface at higher TiO_2 contents. TiO_2 aggregation would reduce the specific surface area and active sites of the photocatalyst and consequently the photodegradation rate.

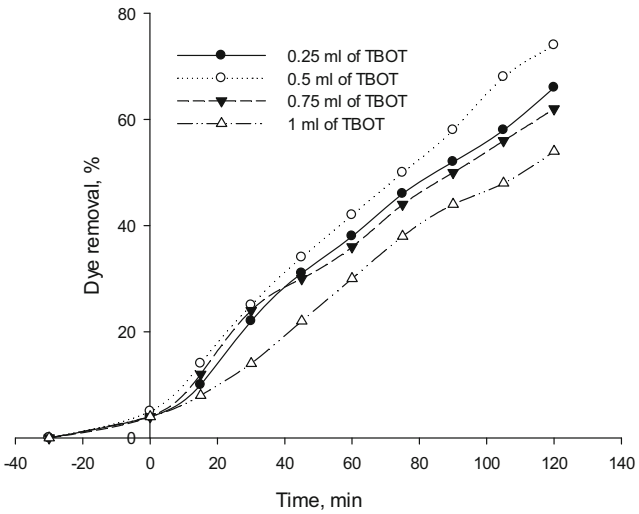

Fig. 14 Effect of TiO_2 loading on RR195 photodegradation using Fe-ZSM-5@TiO_2-Ag (initial dye concentration of 50 mL/L, pH of 3, photocatalyst concentration of 300 mg/L and 0.5 mL of 0.1 M $AgNO_3$)

The heterogeneous photocatalytic oxidation mechanism using Fe-ZSM-5@TiO_2-Ag can be explained as follows [67, 68]. The relevant reactions formula of high photocatalytic activities of Fe-ZSM-5@TiO_2-Ag nanocomposite under natural sunlight irradiation are shown as following:

Under natural sunlight irradiation, a photoelectron is promoted from the filled VB of both TiO_2 and Ag nanoparticles to the empty CB creating a $h^+_{(VB)}$ in the VB and $e^-_{(CB)}$ in the CB according to Eqs. (2) and (3).

$$TiO_2 + \text{Natural Sunlight} \rightarrow TiO_2(e_{CB} + h_{VB}{}^+) \quad (2)$$

$$Ag + \text{Natural Sunlight} \rightarrow Ag(e_{CB} + h_{VB}{}^+) \quad (3)$$

The photogenerated electrons and holes in TiO_2 and Ag then react with water to produce reactive hydroxyl radical ($OH^{\bullet}$) followed by Eqs. (4), (5), (6), (7) and (8). Generally, most of electrons–holes pairs recombine rapidly on the surface of the pure TiO_2 nanostructure while Ag nanoparticles on the surface of Fe-ZSM-5@TiO_2-Ag capture electrons effectively and prevent the electron-hole recombination.

$$H_2O_{(ads)} + h_{VB}{}^+ \rightarrow OH^{\bullet}{}_{(ads)} + H^+{}_{(ads)} \quad (4)$$

$$O_2 + e_{CB} \rightarrow O_2{}^{\bullet}{}_{(ads)} \quad (5)$$

$$O_2{}^{\bullet}{}_{(ads)} + H^+ \leftrightarrow HOO^{\bullet}{}_{(ads)} \quad (6)$$

$$2HOO^{\bullet}{}_{(ads)} \rightarrow H_2O_{2(ads)} + O_2 \quad (7)$$

$$H_2O_{2(ads)} \rightarrow 2OH^{\bullet}{}_{(ads)} \quad (8)$$

The $OH^{\bullet}$ radical formed on the Fe-ZSM-5@TiO_2-Ag surface is an extremely powerful oxidizing agent. It attacks RR195 dye causing it to mineralize.

$$RR195 + OH^{\bullet} \rightarrow CO_2 + H_2O \text{ (dye intermediates)} \quad (9)$$

$$RR195 + h_{VB}{}^{+} \rightarrow \text{oxidation products} \quad (10)$$

$$RR195 + e_{CB} \rightarrow \text{reduction products} \quad (11)$$

Recycling studies

Recycling experiments were conducted under optimum conditions to examine Fe-ZSM-5@TiO_2-Ag photocatalyst stability. To this aim, the photocatalyst particles were separated at the end of the 3rd cycle by allowing them to settle for 90 min. After filtering and washing them, they were calcined at 500 °C for 3 h. The photocatalyst was then re-used for the dye removal by keeping the other reaction conditions constant. The results are presented in Fig. 15. At the end of the 2nd and 3rd cycles, the percentage of the dye removal was observed to be slightly decreased, which could be explained by the accumulation of by-products, such as organic intermediates, in the cavities and on the active sites of the photocatalyst surface after their formations, thus decreasing its activity by increasing organic pollutant adsorption [30]. These results were clearly indicative of the photocatalyst stability and reusability for several cycles of environmentally friendly treatments without losing its original activity in the relevant industries.

Conclusion

The hybrid materials based on Fe-zsm-5 zeolite and Ag-doped TiO_2 were successfully synthesized. Accordingly, a high-purity synthetic photocatalyst with a specific surface area of 332 m^2/g was produced. XRD results indicated the coexistence of Ag and TiO_2 phases. The presence of the anatase form of Ag-doped TiO_2 onto zeolite was confirmed. The TEM measurements showed the formations of the nanocomposites with the diameter sizes of 50–100 nm. TiO_2 bounded to zeolite network by Ti-O and Ti-O-Ag was evidenced via the FT-IR spectra, which further indicated more durable loading of TiO_2 onto zeolite rather than a simple physical combination. The slight shifting of the absorption bands of Ag-doped TiO_2 nanocrystals onto Fe-ZSM-5 zeolite were slightly shifted towards the visible range was exhibited by the UV-Vis spectra, resulting in a stronger response of sunlight.

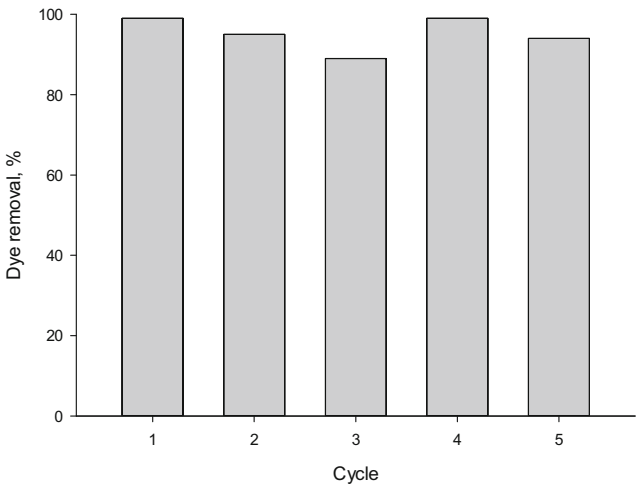

Fig. 15 Dye removal as a function of the number cycle for the Fe-ZSM-5@TiO_2-Ag photocatalyst (initial dye concentration of 50 mL/L, pH of 3, photocatalyst concentration of 300 mg/L after 120 min)

Maximum dye removal (98%) was obtained under the optimum conditions of the photocatalyst concentration (400 mg/L), pH value (3), and sunlight exposure time (90 min) under ambient temperature after 120 min under natural sunlight by using 0.5 ml of TiO_2 and silver ammonium nitrate. Furthermore, by increasing the content of TiO_2 up to 0.5 mL, its photocatalytic activity was enhanced under natural sunlight irradiation. This enhancement was related to the most important role of TiO_2 doping. In fact, the photocatalytic activity was ameliorated by facilitating a longer charge separation through Ag-doped TiO_2 NPs and trapping the photogenerated electrons under sunlight irradiation. Introducing TiO_2 NPs to Ag nanostructure under visible sunlight led to their synergistic effects on the thermocatalytic activity and efficient transmission of electrons at the Ag/TiO_2 interface, thus enhancing the photocatalytic activity of Ag-doped TiO_2 nanocatalyst. In conclusion, this novel Ag-doped TiO_2-Fe-ZSM-5 nanocomposite with sunlight sensitivity can be a promising candidate to purify wastewater containing organic pollutants. Furthermore, the synthesized photocatalyst was found to be stable and reusable for several times with high efficiency under sunlight.

Acknowledgements The study was funded by Tarbiat Modares University (TMU). The authors wish to thank Mrs. Haghdoust for her assistant (Technical Assistant of Environmental Laboratory) and Tarbiat Modares University, Ministry of Science and National Science Foundation for their financial support.

Compliance with ethical standards

Conflict of interest The authors declare that there is no conflict of interest.

References

1. Hou H, Zhou R, Wu P, Wu L. Removal of Congo red dye from aqueous solution with hydroxyapatite/chitosan composite. Chem Eng J. 2012;211-212:336–42.
2. Fouladi Fard R, Sar MEK, Fahiminia M, Mirzaei N, Yousefi N, Mansoorian HJ, et al. Efficiency of multi walled carbon nanotubes for removing direct blue 71 from aqueous solutions. Eurasian J Anal Chem. 2018;13.
3. Jirasripongpun K, Nasanit R, Niruntasook J, Chotikasatian B. Decolorization and degradation of CI reactive red 195 by Enterobacter sp. Sci Technol Asia. 2007:6–11.

4. Elwakeel KZ, Rekaby M. Efficient removal of reactive black 5 from aqueous media using glycidyl methacrylate resin modified with tetraethelenepentamine. J Hazard Mater. 2011;188:10–8.
5. He X, Male KB, Nesterenko PN, Brabazon D, Paull B, Luong JH. Adsorption and desorption of methylene blue on porous carbon monoliths and nanocrystalline cellulose. ACS Appl Mater Interfaces. 2013;5:8796–804.
6. Dalvand A, Nabizadeh R, Reza Ganjali M, Khoobi M, Nazmara S, Hossein Mahvi A. Modeling of reactive blue 19 azo dye removal from colored textile wastewater using L-arginine-functionalized Fe3O4 nanoparticles: optimization, reusability, kinetic and equilibrium studies. J Magn Magn Mater. 2016;404:179–89.
7. Ashrafi SD, Kamani H, Soheil Arezomand H, Yousefi N, Mahvi AH. Optimization and modeling of process variables for adsorption of basic blue 41 on NaOH-modified rice husk using response surface methodology. Desalin Water Treat. 2016;57:14051–9.
8. Kamranifar M, Khodadadi M, Samiei V, Dehdashti B, Noori Sepehr M, Rafati L, et al. Comparison the removal of reactive red 195 dye using powder and ash of barberry stem as a low cost adsorbent from aqueous solutions: isotherm and kinetic study. J Mol Liq. 2018;255:572–7.
9. Ashrafi SD, Rezaei S, Forootanfar H, Mahvi AH, Faramarzi MA. The enzymatic decolorization and detoxification of synthetic dyes by the laccase from a soil-isolated ascomycete, Paraconiothyrium variabile. Int Biodeterior Biodegrad. 2013;85:173–81.
10. Kamani H, Safari GH, Asgari G, Ashrafi SD. Data on modeling of enzymatic elimination of direct red 81 using response surface methodology. Data Brief. 2018;18:80–6.
11. Mehrabian F, Kamani H, Safari GH, Asgari G, Ashrafi SD. Direct blue 71 removal from aqueous solution by laccase-mediated system; a dataset. Data Brief. 2018;19:437–43.
12. Bali U, Çatalkaya E, Şengül F. Photodegradation of reactive black 5, direct red 28 and direct yellow 12 using UV, UV/H 2 O 2 and UV/H 2 O 2/Fe 2+: a comparative study. J Hazard Mater. 2004;114:159–66.
13. Alaton IA, Balcioglu IA, Bahnemann DW. Advanced oxidation of a reactive dyebath effluent: comparison of O 3, H 2 O 2/UV-C and TiO 2/UV-A processes. Water Res. 2002;36:1143–54.
14. X.-H. Qi, Y.-Y. Zhuang, Y.-C. Yuan, W.-X. Gu, Decomposition of aniline in supercritical water. J Hazard Mater, 90 (2002) 51–62.
15. Madhavan J, Maruthamuthu P, Murugesan S, Anandan S. Kinetic studies on visible light-assisted degradation of acid red 88 in presence of metal-ion coupled oxone reagent. Appl Catal B Environ. 2008;83:8–14.
16. R.A. Al-Rasheed, Water treatment by heterogeneous photocatalysis an overview. In: 4th SWCC acquired experience symposium held in Jeddah, 2005, pp. 1–14.
17. Hemmati Borji S, Nasseri S, Mahvi AH, Nabizadeh R, Javadi AH. Investigation of photocatalytic degradation of phenol by Fe(III)-doped TiO2 and TiO2 nanoparticles. J Environ Health Sci Eng. 2014;12:101.
18. Safari GH, Hoseini M, Seyedsalehi M, Kamani H, Jaafari J, Mahvi AH. Photocatalytic degradation of tetracycline using nanosized titanium dioxide in aqueous solution. Int J Environ Sci Technol. 2015;12:603–16.
19. Kaur S, Singh V. TiO 2 mediated photocatalytic degradation studies of reactive red 198 by UV irradiation. J Hazard Mater. 2007;141:230–6.
20. Soutsas K, Karayannis V, Poulios I, Riga A, Ntampegliotis K, Spiliotis X, et al. Decolorization and degradation of reactive azo dyes via heterogeneous photocatalytic processes. Desalination. 2010;250:345–50.
21. Poulios I, Tsachpinis I. Photodegradation of the textile dye reactive black 5 in the presence of semiconducting oxides. J Chem Technol Biotechnol. 1999;74:349–57.
22. Li F, Sun S, Jiang Y, Xia M, Sun M, Xue B. Photodegradation of an azo dye using immobilized nanoparticles of TiO 2 supported by natural porous mineral. J Hazard Mater. 2008;152:1037–44.
23. Shankar M, Anandan S, Venkatachalam N, Arabindoo B, Murugesan V. Fine route for an efficient removal of 2, 4-dichlorophenoxyacetic acid (2, 4-D) by zeolite-supported TiO 2. Chemosphere. 2006;63:1014–21.
24. Yoneyama H, Torimoto T. Titanium dioxide/adsorbent hybrid photocatalysts for photodestruction of organic substances of dilute concentrations. Catal Today. 2000;58:133–40.
25. Matthews RW. Kinetics of photocatalytic oxidation of organic solutes over titanium dioxide. J Catal. 1988;111:264–72.
26. Seery MK, George R, Floris P, Pillai SC. Silver doped titanium dioxide nanomaterials for enhanced visible light photocatalysis. J Photochem Photobiol A Chem. 2007;189:258–63.
27. Fujishima A, Zhang X, Tryk DA. TiO2 photocatalysis and related surface phenomena. Surf Sci Rep. 2008;63:515–82.
28. Teh CM, Mohamed AR. Roles of titanium dioxide and ion-doped titanium dioxide on photocatalytic degradation of organic pollutants (phenolic compounds and dyes) in aqueous solutions: a review. J Alloys Compd. 2011;509:1648–60.
29. Yang X, Ma F, Li K, Guo Y, Hu J, Li W, et al. Mixed phase titania nanocomposite codoped with metallic silver and vanadium oxide: new efficient photocatalyst for dye degradation. J Hazard Mater. 2010;175:429–38.
30. Ghasemi Z, Younesi H, Zinatizadeh AA. Preparation, characterization and photocatalytic application of TiO 2/Fe-ZSM-5 nanocomposite for the treatment of petroleum refinery wastewater: optimization of process parameters by response surface methodology. Chemosphere. 2016;159:552–64.
31. Ghasemi Z, Younesi H, Zinatizadeh AA. Kinetics and thermodynamics of photocatalytic degradation of organic pollutants in petroleum refinery wastewater over nano-TiO2 supported on Fe-ZSM-5. J Taiwan Inst Chem Eng. 2016;65:357–66.
32. Yan G, Wang X, Fu X, Li D. A primary study on the photocatalytic properties of HZSM-5 zeolite. Catal Today. 2004;93–95:851–6.
33. Ohno T, Murakami N, Tsubota T, Nishimura H. Development of metal cation compound-loaded S-doped TiO2 photocatalysts having a rutile phase under visible light. Appl Catal A Gen. 2008;349:70–5.
34. Huang X, Wang G, Yang M, Guo W, Gao H. Synthesis of polyaniline-modified Fe3O4/SiO2/TiO2 composite microspheres and their photocatalytic application. Mater Lett. 2011;65:2887–90.
35. M.M. Treacy, J.B. Higgins, Collection of simulated XRD powder patterns for zeolites fifth (5th) revised edition, Elsevier, 2007.
36. Geetha D, Kavitha S, Ramesh P. A novel bio-degradable polymer stabilized ag/TiO 2 nanocomposites and their catalytic activity on reduction of methylene blue under natural sun light. Ecotoxicol Environ Saf. 2015;121:126–34.
37. Xue C-H, Chen J, Yin W, Jia S-T, Ma J-Z. Superhydrophobic conductive textiles with antibacterial property by coating fibers with silver nanoparticles. Appl Surf Sci. 2012;258:2468–72.
38. Kumar R, El-Shishtawy R, Barakat M. Synthesis and characterization of ag-Ag2O/TiO2@polypyrrole heterojunction for enhanced photocatalytic degradation of methylene blue. Catalysts. 2016;6:76.
39. Chong MN, Tneu ZY, Poh PE, Jin B, Aryal R. Synthesis, characterisation and application of TiO2–zeolite nanocomposites for the advanced treatment of industrial dye wastewater. J Taiwan Inst Chem Eng. 2015;50:288–96.
40. Reporting Physisorption Data for Gas/Solid Systems. In: Handbook of Heterogeneous Catalysis.
41. Sakthivel S, Neppolian B, Shankar MV, Arabindoo B, Palanichamy M, Murugesan V. Solar photocatalytic degradation of azo dye: comparison of photocatalytic efficiency of ZnO and TiO2. Sol Energy Mater Sol Cells. 2003;77:65–82.

42. Sobana N, Muruganadham M, Swaminathan M. Nano-ag particles doped TiO2 for efficient photodegradation of direct azo dyes. J Mol Catal A Chem. 2006;258:124–32.
43. Miecznikowski A, Hanuza J. Infrared and Raman studies of ZSM-5 and silicalite-1 at room, liquid nitrogen and helium temperatures. Zeolites. 1987;7:249–54.
44. Sundaramurthy V, Lingappan N. Isomorphic substitution of boron in ZSM-5 type zeolites using TBP as template. J Mol Catal A Chem. 2000;160:367–75.
45. Li F, Jiang Y, Yu L, Yang Z, Hou T, Sun S. Surface effect of natural zeolite (clinoptilolite) on the photocatalytic activity of TiO2. Appl Surf Sci. 2005;252:1410–6.
46. Liu X, Iu K-K, Kerry Thomas J. Encapsulation of TiO2 in zeolite Y. Chem Phys Lett. 1992;195:163–8.
47. Hansen JØ, Lira E, Galliker P, Wang J-G, Sprunger PT, Li Z, et al. Enhanced bonding of silver nanoparticles on oxidized TiO2(110). J Phys Chem C. 2010;114:16964–72.
48. Tom RT, Nair AS, Singh N, Aslam M, Nagendra CL, Philip R, et al. Freely dispersible au@TiO2, au@ZrO2, ag@TiO2, and ag@ZrO2 Core−Shell nanoparticles: one-step synthesis, characterization, spectroscopy, and optical limiting properties. Langmuir. 2003;19:3439–45.
49. Zainudin NF, Abdullah AZ, Mohamed AR. Characteristics of supported nano-TiO 2/ZSM-5/silica gel (SNTZS): photocatalytic degradation of phenol. J Hazard Mater. 2010;174:299–306.
50. Xie C, Xu Z, Yang Q, Xue B, Du Y, Zhang J. Enhanced photocatalytic activity of titania–silica mixed oxide prepared via basic hydrolyzation. Mater Sci Eng B. 2004;112:34–41.
51. Rajeshwar K, Osugi ME, Chanmanee W, Chenthamarakshan CR, Zanoni MVB, Kajitvichyanukul P, et al. Heterogeneous photocatalytic treatment of organic dyes in air and aqueous media. J Photochem Photobiol C: Photochem Rev. 2008;9:171–92.
52. Hoffmann MR, Martin ST, Choi W, Bahnemann DW. Environmental applications of semiconductor Photocatalysis. Chem Rev. 1995;95:69–96.
53. Moradi N, Amin MM, Fatehizadeh A, Ghasemi Z. Degradation of UV-filter Benzophenon-3 in aqueous solution using TiO2 coated on quartz tubes. J Environ Health Sci Eng. 2018;16:213–28.
54. Sahel K, Perol N, Chermette H, Bordes C, Derriche Z, Guillard C. Photocatalytic decolorization of Remazol black 5 (RB5) and Procion red MX-5B—isotherm of adsorption, kinetic of decolorization and mineralization. Appl Catal B Environ. 2007;77:100–9.
55. Ashrafi SD, Kamani H, Mahvi AH. The optimization study of direct red 81 and methylene blue adsorption on NaOH-modified rice husk. Desalin Water Treat. 2016;57:738–46.
56. Konstantinou IK, Albanis TA. TiO2-assisted photocatalytic degradation of azo dyes in aqueous solution: kinetic and mechanistic investigations: a review. Appl Catal B Environ. 2004;49:1–14.
57. Barakat MA. Adsorption and photodegradation of Procion yellow H-EXL dye in textile wastewater over TiO2 suspension. J Hydro Environ Res. 2011;5:137–42.
58. Behnajady M, Modirshahla N, Hamzavi R. Kinetic study on photocatalytic degradation of CI acid yellow 23 by ZnO photocatalyst. J Hazard Mater. 2006;133:226–32.
59. Kamani H, Bazrafshan E, Ashrafi SD, Sancholi F. Efficiency of Sono-nano-catalytic process of Tio2 Nano-particle in removal of erythromycin and metronidazole from aqueous solution. Journal of Mazandaran University of Medical. Sciences. 2017;27:140–54.
60. Kalhor MM, Rafati AA, Rafati L, Rafati AA. Synthesis, characterization and adsorption studies of amino functionalized silica nano hollow sphere as an efficient adsorbent for removal of imidacloprid pesticide. J Mol Liq. 2018;266:453–9.
61. Sauer T, Cesconeto Neto G, José HJ, Moreira RFPM. Kinetics of photocatalytic degradation of reactive dyes in a TiO2 slurry reactor. J Photochem Photobiol A Chem. 2002;149:147–54.
62. Wu C-H. Comparison of azo dye degradation efficiency using UV/single semiconductor and UV/coupled semiconductor systems. Chemosphere. 2004;57:601–8.
63. Daneshvar N, Rabbani M, Modirshahla N, Behnajady MA. Kinetic modeling of photocatalytic degradation of acid red 27 in UV/TiO2 process. J Photochem Photobiol A Chem. 2004;168:39–45.
64. Pelaez M, Nolan NT, Pillai SC, Seery MK, Falaras P, Kontos AG, et al. A review on the visible light active titanium dioxide photocatalysts for environmental applications. Appl Catal B Environ. 2012;125:331–49.
65. Yurdakal S, Tek BS, Değirmenci Ç, Palmisano G. Selective photocatalytic oxidation of aromatic alcohols in solar-irradiated aqueous suspensions of Pt, au, Pd and ag loaded TiO2 catalysts. Catal Today. 2017;281:53–9.
66. Damm C, Herrmann R, Israel G, Müller FW. Acrylate photopolymerization on heterostructured TiO2 photocatalysts. Dyes Pigments. 2007;74:335–42.
67. Geetha D, Kavitha S, Ramesh PS. A novel bio-degradable polymer stabilized ag/TiO2 nanocomposites and their catalytic activity on reduction of methylene blue under natural sun light. Ecotoxicol Environ Saf. 2015;121:126–34.
68. Ajmal A, Majeed I, Malik RN, Idriss H, Nadeem MA. Principles and mechanisms of photocatalytic dye degradation on TiO2 based photocatalysts: a comparative overview. RSC Adv. 2014;4:37003–26.